International Journal of Steel Structures
December 2014, Vol 14, No 4, 683-695
DOI 10.1007/s13296-014-1201-3

International Journal of
STEEL
STRUCTURES
www.springer.com/journal/13296

Seismic Design, Nonlinear Analysis, and Performance Evaluation of Recentering Buckling-restrained Braced Frames (BRBFs)

Jong-Wan Hu[1,2] and Eunsoo Choi[3,*]

[1]*Assistant Professor, Department of Civil and Environmental Engineering, College of Urban Science, Incheon National University, Incheon, 406-840, Korea*
[2]*Head of Center, Incheon Disaster Prevention Research Center, Incheon National University, 12-1 Songdo-dong, Yeonsu-gu, Incheon, 406-840, Korea*
[3]*Associate Professor, Department of Civil Engineering, Hongik University, Seoul, 121-791, Korea*

Abstract

Buckling-restrained braced frames (BRBFs) have been increasingly used as seismic-load resisting systems in the area of high seismicity due to the fact that their performance is far superior to that of concentrically braced frames (CBFs). The buckling-restrained brace (BRB) members have inherent ability to yield under both tension and compression without buckling, but large strains that can make entire frame structures more prone to permanent deformation intensively occurs at the end support connector. This dilemma can be solved applying auto-restoration capability to this part of the bracing member. For this reason, this study suggests a methodology that incorporates recentering systems obtained by utilizing superelastic shape memory alloys (SMAs) into buckling-restrained braces (BRBs). The superelastic SMAs recover original configuration without heat treatment even after experiencing large deformation. Analytical frame models are developed to evaluate the BRBFs with respect to peak and residual inter-story drifts. The analytical findings demonstrate that, compared to frames with conventional steel bracing systems, the BRBFs with superelastic SMA bracing systems are able to reduce residual inter-story drifts more effectively during earthquake events due to the self-healing characteristics of such SMA materials.

Keywords: shape memory alloys (SMAs), superelastic behavior, buckling-restrained braced frames (BRBFs), nonlinear dynamic analyses, residual inter-story drifts, stress hinges

1. Introduction

Buckling-restrained braced frames (BRBFs) are newly developed framing systems characterized by the use of diagonal braces that are designed to yield during both tension and compression (Watanabe *et al*., 1988; Black *et al*., 2002; Aiken *et al*., 2002; Inoue *et al*., 2001). Despite being a relatively new type of braced system, the BRBFs that can preclude brace buckling in compression have been currently recognized as an alternative approach to concentrically braced frames (CBFs) conventionally used for steel construction. Buckling-restrained braces (BRBs) have fully balanced hysteresis loops with compression-yielding close to tension-yielding behavior, thereby providing stable energy dissipation at the high seismic ground motions (Sabelli, 2004; Wada *et al*., 1992; Kim *et al*., 2009). In addition, BRBFs exhibit high lateral stiffness as compared to conventional moment-resisting frames, making it easy to meet drift requirements specified in the current design code (Guo *et al*., 2011; Kim *et al*., 2004). Therefore, they are clearly more profitable than other steel frame structures.

The BRBs act as a supplemental fuse, which is designed to gather acceptable damage in the entire structure, and it is possible to replace damaged braces with new ones after major seismic events (Wada *et al*., 1992; Park *et al*., 2011). The BRBs contribute to minimizing failure to other main frame members in that braced frame structures can partially recover their original conditions by virtue of this damage tolerant brace member. Nevertheless, permanent deformation typically taking place in the bracing member intends to incur an increase in the residual inter-story drift of the entire frame structure. In that case, extra costs will be inevitable to restore the laterally deformed entire structure to its original state. Even though replacing work on the bracing system is demanded only for repair, distinct criteria for changing the impaired braces need to

Note.-Discussion open until May 1, 2015. This manuscript for this paper was submitted for review and possible publication on February 4, 2014; approved on December 1, 2014.

*Corresponding author
Tel: +82-2-320-3060; Fax: +82-2-332-1244
E-mail: eunsoochoi@hongik.ac.kr

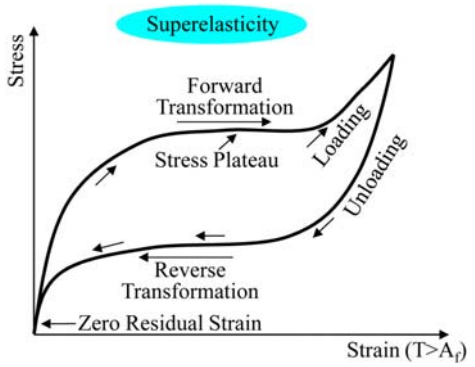

Figure 1. Stress-strain behavior of superelastic SMA materials.

be established instead of depending on engineer's subjective decisions. Accordingly, in this study, the recentering mechanism should be introduced to the bracing system so as to greatly decrease permanent deformation caused by mid- to high-level seismic events.

Recentering devices recognized as seismic retrofitting systems have received increasing attention, especially in the US and Japan (Song *et al*., 2006). One significant method to obtain recentering capabilities is to utilize smart materials which can be integrated into frame structures. Superelastic shape memory alloys (SMAs) are a good example of such promising smart materials due to their self-healing characteristics achieved by only load removal. An idealized plot of the stress-strain relationships in the superelastic SMAs is presented in Fig. 1. As can be seen in this figure, superelastic (or austenitic) behavior referred to as a flag-shape hysteresis with zero residual strain upon unloading occur for temperatures above the austenite finish temperature (A_f). The zero residual strain of austenitic phase SMAs is expected to gain a range of up to 8 percent strain (DesRoches *et al*., 2004). In addition to repeatable recentering capabilities provided by the superelastic effect, their properties include supplemental damping attributed to the flag-shape hysteresis, stress plateaus to limit force transmission at intermediate strain levels, stress stiffening at large strain levels, excellent corrosion resistance, outstanding fatigue properties, and others (Song *et al*., 2006; DesRoches *et al*., 2004).

Many researchers have explored the application of SMAs in civil structures, and, in particular, their efforts have recently extended to using SMA tendons as active damage control devices in the bolted connections (Ocel *et al*., 2004; Hu, 2008; Hu *et al*., 2010, 2011, 2012; Hu and Leon, 2011). In the behavior of the whole building, SMA tendon connections constructed in moment-resisting frames contribute to both establishing additional damping and mitigating residual story drifts. Besides, SMA energy dissipation devices used for passive control of civil structures have been seen in the form of diagonal braces. This practical application takes advantage of excellent damping properties, which are attributed to their hysteretic behavior under dynamic loading (Dolce and Cardone, 2001; DesRoches and Delemont, 2002).

Synthesizing the above ideas, it is clear that one of the best ways for the purpose of ameliorating the seismic performance of braced frame systems is to apply smart materials to a part of the BRB member. Thus, this study proposes a new innovative structure for BRBFs with superelastic SMA bracing systems, aiming at achieving not only superior recentering behavior but also supplemental energy dissipation. Once superelastic SMA bars used in the place of steel bars are installed at a part of where plastic deformation is likely to converge (e.g., connector between the brace and the frame), braced frames make the best use of recentering capabilities. The primary purpose of this study is to appraise the seismic performance of both BRBFs with superelastic SMA bracing systems and those with conventional steel bracing systems in terms of residual inter-story drifts and recentering ratios through a series of nonlinear time-history dynamic analyses. The analytical results for two BRBF types are compared in an effort to demonstrate that SMAs can be effective in mitigating damages during seismic events.

2. Design of BRB Frame

In accordance with ASCE 7-05 (ASCE, 2005) and IBC 2006 specifications (ICC, 2006), all of the frame buildings presented herein were designed to be an ordinary office building located on a stiff soil site (site class D per ASCE 7-05 definition) in the Los Angeles area, assuming a seismic hazard of 10% probability of exceedance in 50 years. Furthermore, the seismic design category (SDC) is considered to be a high seismicity area as specified for class D in the ASCE 7-05. The other basic conditions used for building design are presented in Table 1.

The prototype buildings were constructed as 6-story frame structures with braced bays along the center of the perimeter to withstand lateral loads. They were designed to be symmetrical in plan with a uniform distribution of mass and stiffness. A plan view of 6-story buildings with five 9.15-m bays is presented in Fig. 2. 6 braced bays, denoted as dashed lines in the figure, were installed in each direction. The perimeter moment-resisting frames required to resist lateral loads are denoted as thick lines in

Table 1. Basic conditions for building design

Located area	Loads (Other)	Loads (Roof)	SDC	Site condition	Occupancy category
LA Area	DL: 4.12 kPa LL: 2.39 kPa	DL: 4.05 kPa LL: 0.96 kPa	D Class	Stiff Soil (Class D)	Ordinary structure

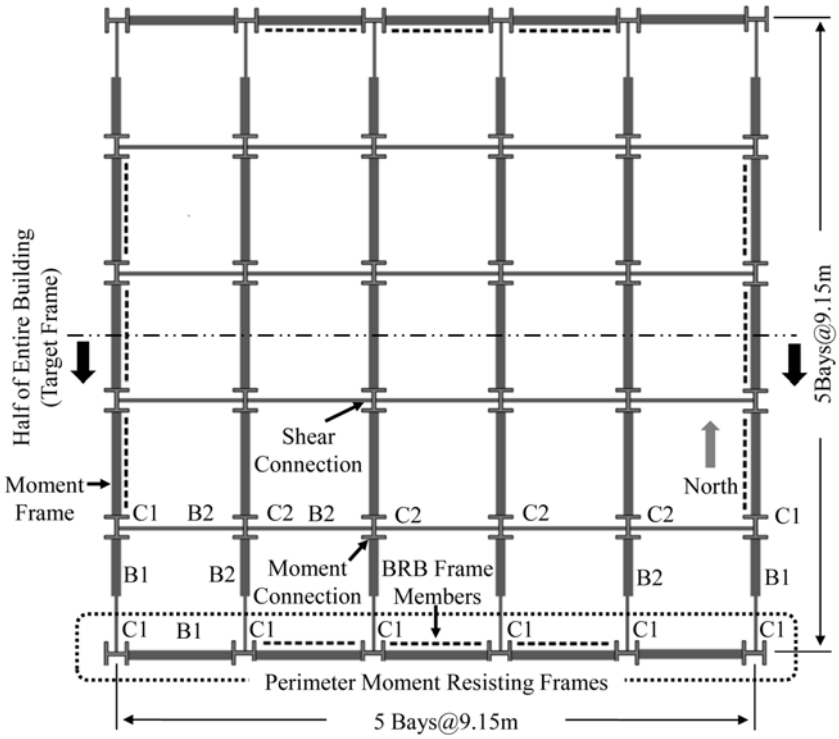

Figure 2. Plan view of six-story building.

the building plan. The gravity-resisting frames connected by simple shear pin connections in interior floor beams head toward the east-west direction. The check on building design was conducted through 2D nonlinear pushover analyses for frame structures that are under essentially regular condition, without in-plane torsional effects.

Inverted V- (chevron), V-, and 2-story X-braced frame systems were selected among the various concentrically braced systems. The elevation views are shown in Fig. 3 for the different types of braced bays, with a detailed drawing of gusset plate connections between BRB members and other main frame members. The first acronym in the model ID (i.e., 6SBRB) indicates 6-story BRBFs. The second acronym represents the type of braced framing system (S: inverted V-braced frame, V: V-braced frame, and 2X: 2 story X-braced frame). Finally, a third acronym is added in case of using superelastic SMA bracing systems. For example, the model ID for a 6-story BRBF with an inverted V-braced framing system is denoted as 6SBRB-S. All of the BRBFs have a uniform story height of 3.96 m. The members of the frame system were designed in accordance with AISC-LRFD manual (AISC, 2001). Column sections are uniform throughout the building height, while, except for the interior floor beams, beam sections for the higher stories were designed with smaller beam sizes, for more economical construction. As presented in Table 2, these member sizes were the same for individual frame models in order to compare each other.

The BRBs consisting of circular metal cores and concrete-filled steel casting tubes were presented in this study. The metal cores encased by steel casing and concrete were fabricated with A572-Gr.50 carbon steel, and hence made it possible to supply the bracing system with high strength and excellent ductility simultaneously. At the lower stories, the encased steel cores designed with larger cross-section areas were installed to resist larger lateral forces in that they function as the primary load-carrying component in the brace member (Table 2). The steel casing of the BRB member was designed with circular shape, and thus fabricated with standard hollow structural section (HSS) tubes available in the current design specification (e.g. HSS6x1/4 made of Gr. B steel) (AISC, 2001).

As can be also shown in Fig. 3, connecting bars made of superelastic SMA or steel materials were installed at both end segments, and then combined in series with the encased steel core of the BRB member. They were designed with the same diameter as the encased steel cores. The composite cross-sections consisting of circular metal cores and concrete-filled steel casting tubes, which results in the main body of the BRB member, behave in a relatively rigid manner to the connecting bars. For this reason, the end connecting bars are vulnerable to undergoing plastic deformations induced by a difference in stiffnesses between two parts.

3. Analytical Models

3.1. Modeling attributes for building structures

The seismic behavior of the BRBFs was examined through

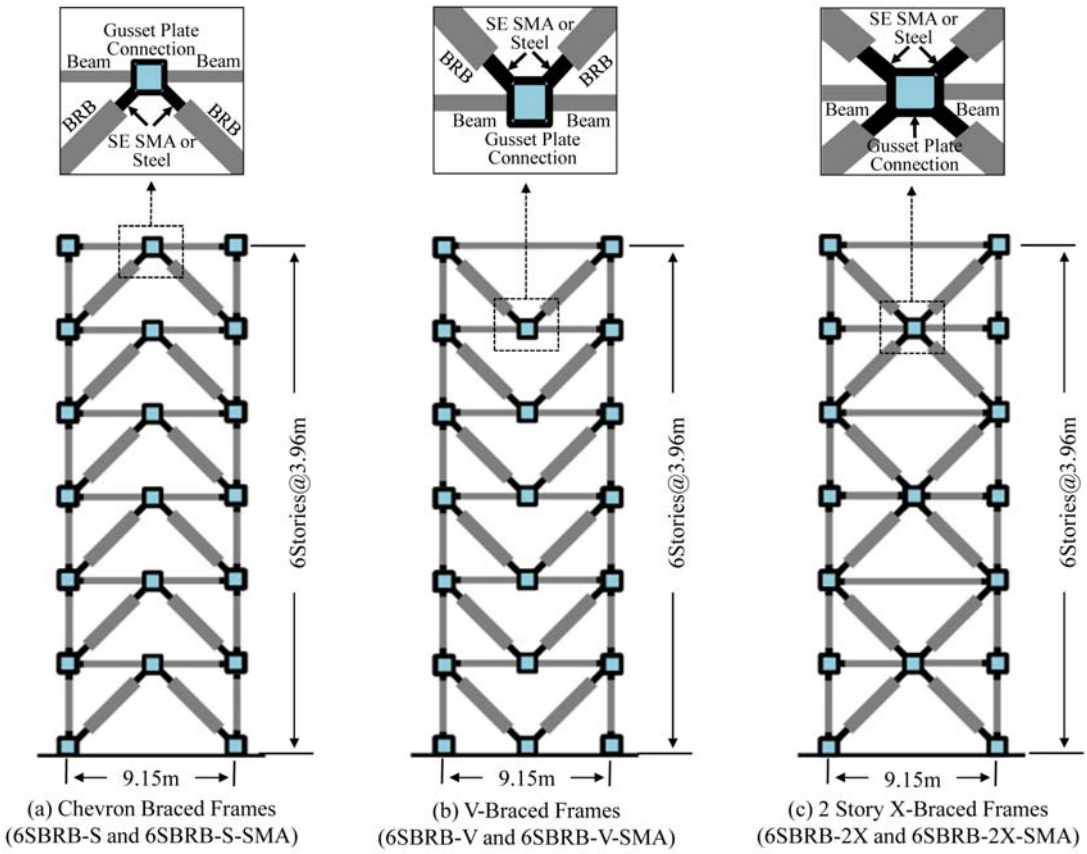

Figure 3. Details and elevation views of BRB Frames installed in six-story building.

nonlinear time-history dynamic analyses performed on 6 frame models. The Open System for Earthquake Engineering Simulation (OpenSEES) (Mazzoni *et al*., 2006) program was used to conduct these analyses. The prototype BRBF buildings considered in this study can be modeled as 2D half symmetric frame models because of their regular quadrilateral configuration. It may not be necessary to consider in-plane torsion effect. Subjected to a ground motion, the modeling attributes for 2D perimeter moment-resisting frames assembled in parallel with inside gravity-resisting frames are shown in Fig. 4. The leaning column members located in the gravity frame are demanded to be subjected to half building weight in the frame model and thus factored dead and live loads were vertically applied to these column members. P-delta effects arising from second-order behavior due to large deformation were taken into consideration for nonlinear analyses.

In order to effectively resist lateral-seismic loads, the building structures were designed with the perimeter frame system enhanced by moment connections and BRB members. The concrete floor slabs connected between two frame systems intend to behave as rigid diaphragms. The lateral behavior of the perimeter moment-resisting frames was consequently followed by that of the gravity-resisting frames. For these reasons, the frame members in the perimeter moment-resisting frame were modeled using

Table 2. Member sizes used in building design

Story	Column* (C1)	Beam* (B1)	BRB		Int. column* (C2)	Int. beam* (B2)
			Core area*(mm^2)	Casing tube**		
1	W14×109	W24×84	2580	HSS6×1/4	W12×87	W24×68
2	W14×109	W24×84	2580	HSS6×1/4	W12×87	W24×68
3	W14×109	W24×84	2580	HSS6×1/4	W12×87	W24×68
4	W14×109	W24×84	2580	HSS6×1/4	W12×87	W24×68
5	W14×109	W18×50	2027	HSS6×1/4	W12×87	W24×68
6	W14×109	W18×50	2027	HSS6×1/4	W12×87	W24×68

*Gr.50 Carbon Steel **Gr.B Carbon Steel

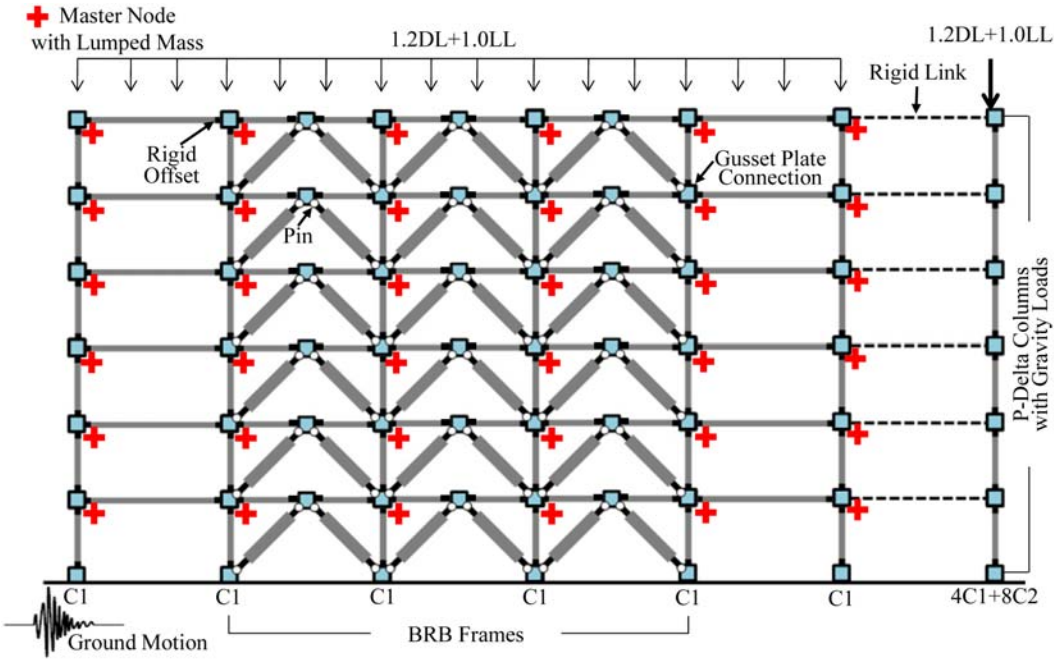

Figure 4. Modeling attributes for 2D frame models.

nonlinear beam-column elements with 2D fiber sections for the purpose of simulating nonlinear material behavior. On the other hand, the leaning column members were modeled as elastic beam-column elements that only depend on the dimension of the column member. In the 2D frame model, the rigid links connecting two frame systems were used to construct single multi-point constraint (MPC) objects which are able to constrain translational degree of freedoms (DOFs) between slave nodes located on the gravity frame and master nodes located on the perimeter moment frame. Accordingly, the behavior of the rigid diaphragm can be reproduced using these MPC objects in the program.

In this study, the P-delta coordinate transformations associated with nonlinear and elastic beam-column elements were used to construct geometric nonlinearities including second-order effects. All steel members possessed the strain hardening ratio of 1.5%. An effective viscous damping coefficient of 5% was applied in accordance with the common practice for code designed steel structures (Sabelli *et al*., 2003). The primary response data included nodal displacements, base shear forces, time periods, and fiber stresses. These were collected by using the recorder commands available in the OpenSEES program.

3.2. BRB modeling

The BRB members were modeled also using nonlinear beam-column elements with 2D fiber sections so as to simulate the material behavior of steel casing tubes and confined concrete. Contrary to the modeling of CBF members, the initial imperfection generally produced by placing the nodal position slightly off-center was not necessary to model the BRB members on the ground to yield under both tension and compression, without buckling. The behavior of the BRB members is determined only by material properties that can be reproduced by uniaxial material commands in the program. The composite sections, which can be modeled as the 2D fiber sections including each of material properties, were assigned to numerical integration points in the nonlinear beam-column element. Fig. 5 shows numerical modeling and hysteretic behavior of the BRB member. As can be seen in the curve, it reaches the yield point under compression owing to the absence of initial imperfection. Moreover, an inherent characteristic of confined concrete can make compressive strength slightly higher in comparison with tensile strength.

The end connecting bars produced by either Gr. 50 steel or superelastic SMA according to the frame models were also modeled as nonlinear beam-column elements (Fig. 5(a)). The simulated curves for these material behaviors are given in Fig. 6. The material behavior of Gr. 50 steel, which is characterized by an elastic modulus of 200 GPa, a yield stress (Fy) of 345 MPa, and a hardening ratio of 1.5%, was simulated using the uniaxial steel material command. The material behavior of the superelastic SMA was simulated using the user-defined material (UMAT) code (Auricchio and Sacco, 1997), because an appropriate default material command was not available in the OpenSEES program. In this study, required material parameters used to simulate the material behavior of superelastic SMAs -elastic modulus (41 GPa), yield stress (413 MPa), recoverable elongation (8%), and ultimate recoverable stress (516 MPa)- were defined based on the

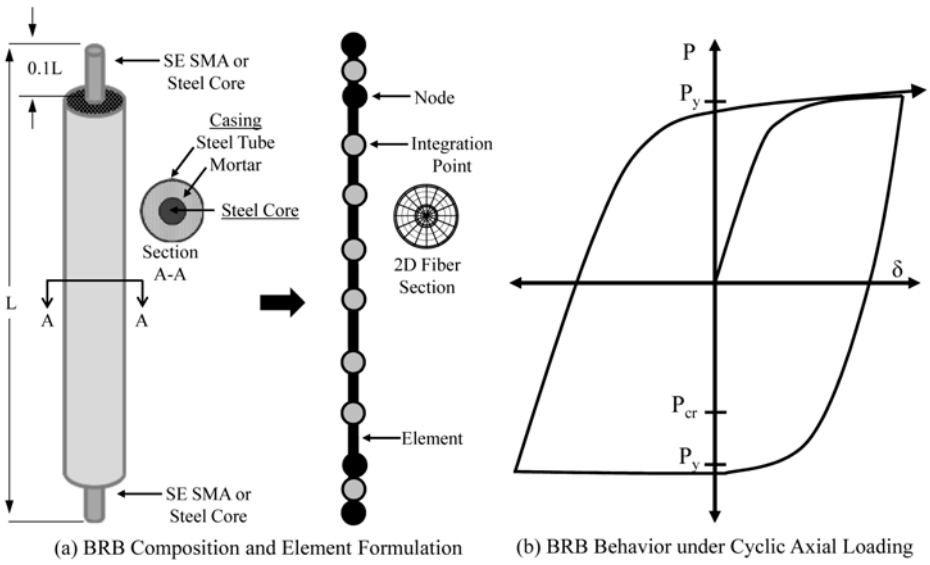

Figure 5. Modeling of BRB frame members.

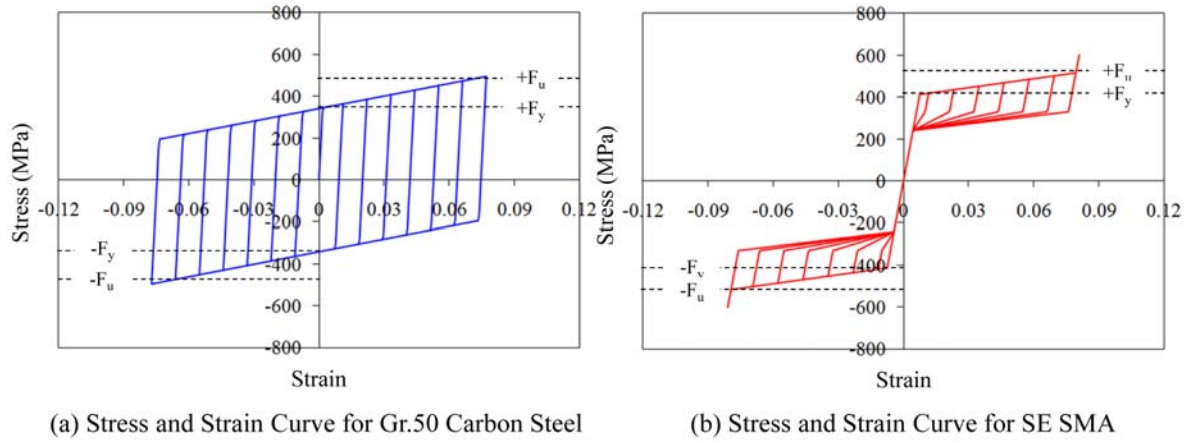

Figure 6. Idealized behavior of Gr.50 carbon steel and SE SMA materials used in BRBs.

results of the uniaxial pull-out test carried out by DesRoches *et al*. (2004) with 25-mm diameter superelastic SMA bars. The superelastic SMA materials commonly have more flexible-elastic modulus and higher post-yield strength than the steel materials.

4. Nonlinear Dynamic Analyses

4.1. Ground motions and other considerations

The ground motions originally developed as a part of the SAC project (Somerville *et al*., 1997) were used in this study. Two different seismic hazard levels of seismic ground motions, (a) the design level earthquake (DLE) associated with a 10% probability of exceedence in 50 years (10% in 50 years) and (b) the maximum credible earthquake (MCE) associated with a 2% probability of exceedence in 50 years (2% in 50 years), were considered to perform a total of 24 nonlinear dynamic analyses. For each seismic hazard level, two types of ground motions, which were classified as short and long period motions (i.e., LA15 and LA17, LA25 and LA27; Fig. 7), were used for obtaining more insight into the seismic behavior of BRB frame models. These ground motion records were scaled to match the design acceleration response spectrum for the L.A. area where the 2D frame models were located, which corresponds to the site class D specified in ASCE 7-05.

In order to solve the time dependent-dynamic problem, transient equilibrium analyses were performed using the Newmark method. The effective damping, as defined by the Rayleigh command in the OpenSEES program, was added to these analyses. To reflect the second order effects (P-Delta effect) arising from dead and live loads along the direction of gravity during the dynamic analyses, equivalent point loads converted from these gravity loads were also applied to the beam elements. In addition to the gravity loads used to model the P-Delta effects, lumped masses were assigned to nodes on the moment-resisting

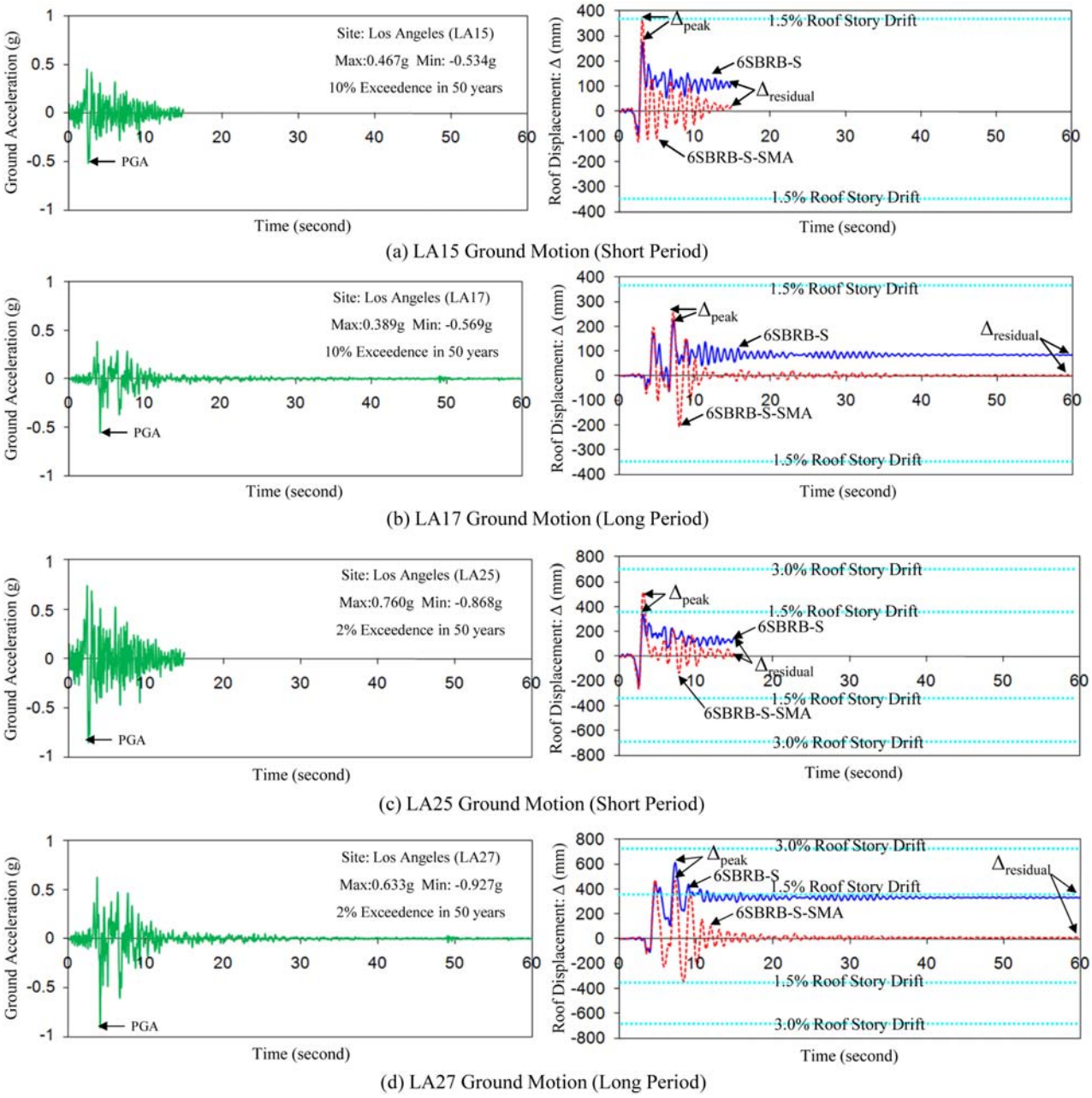

Figure 7. Results of nonlinear dynamic analyses (roof story displacement vs. time).

frames (Fig. 4) so as to generate the story shear forces resulting from ground acceleration. Lumped masses were made up of 1.0 times dead loads plus 0.2 times live loads.

4.2. Nonlinear dynamic analysis results

The seismic responses of SMA-braced frames are compared with those of steel-braced frames through nonlinear dynamic time-history analyses, using 4 ground motion records. The LA15 ground motion has relatively short duration (15 seconds), with a peak ground acceleration (PGA) value of 0.534 g, while the LA17 ground motion has relatively long duration (60 seconds) with a PGA value of 0.569 g. Both ground motions belong to a seismic hazard level of 10% probability of exceedence in 50 years. For a seismic hazard level of 2% probability of exceedence in 50 years, the LA25 ground motion has 15-second duration with a PGA value of 0.868 g, and the LA27 ground motion has 60-second duration with a PGA value of 0.927 g. Including these ground motion data, the corresponding time-histories for the roof story displacement of both compared frame models are provided in Fig. 7. The resulting curves for roof story drifts versus base shear forces are also presented in Fig. 8.

Under the relatively weak ground motions (i.e., 10% in 50 year seismic hazard level), the BRBF models with superelastic bracing systems generally exhibited larger

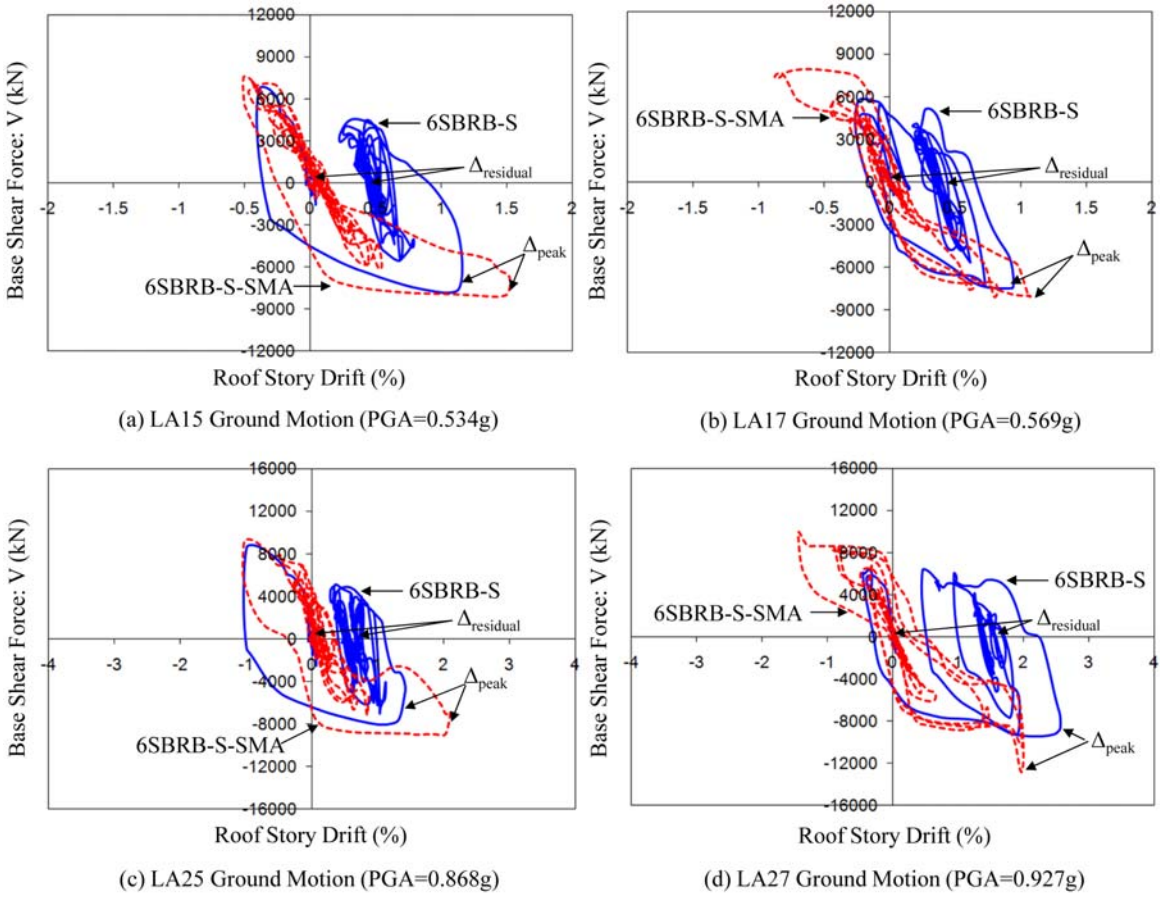

Figure 8. Results of nonlinear dynamic analyses (roof story drift vs. base shear force).

peak roof displacements than those with conventional steel bracing systems because the behavior of SMA materials is more flexible as regards the elastic modulus than that of steel materials. For instance, the peak displacements for the 6SBRB-S-SMA and 6SBRB-S frame model subjected to the LA15 ground motion were 356 and 259 mm, respectively, values that indicate the roof story drifts of 1.50 and 1.09%.

However, under the relatively strong ground motions (i.e., 2% in 50 year seismic hazard level), the peak roof displacements of both BRB frame models exceeded the 1.5% roof story drift limit. The stress stiffening displayed by superelastic SMA elements at a high large strain level enables the SMA-braced frame model to accommodate more lateral base shear forces after the post-yield state has quite progressed. Hence, under the LA27 ground motion considered as one of the most strong seismic excitations, the 6SBRB-S-SMA frame model showed the smaller peak roof displacement than the 6SBRB-S frame model (Figs. 7(d) and 8(d)). In addition, as shown in Fig. 8, the 6SBRB-S-SMA frame model have larger base shear forces overall when the peak roof displacements occur. As can be seen in both figures, superelastic SMA bracing systems significantly contribute to reducing the residual roof displacement. Their excellent damping properties also help to quickly decrease the amplitude of roof displacements during ground motions as well.

The peak and residual responses were investigated to examine the dynamic performance of the BRBF models. The analysis results for inter-story drifts under the peak roof story drifts, and the residual inter-story drifts for all BRBF models, in response to the different ground motions used, are summarized in Table 3. The occurrence time of each peak roof displacement was almost same for both BRBF models being compared under the same ground motion, and lagged behind the PGA time by about 2 to 3 seconds. After the LA27 ground motion, the residual roof displacement of the 6SBRB-S frame model was as much as 37 times that of the 6SBRB-S-SMA frame model (i.e., approximately 330 mm). Therefore, the ability of superelastic SMA bracing systems to restore a braced frame to its original condition can be expected to considerably mitigate the permanent deformation of the entire frame building. Overall, larger post-yield shear forces were observed at the seismic behavior of the 6SBRB-S-SMA frame model (Table 3).

4.3. Seismic evaluation

Based on the analysis results, the corresponding recentering ratios are presented in Table 4. The maximum values of

Table 3. Summary of ultimate and residual inter-story drifts obtained from nonlinear dynamic analyses

Model ID	Inter-story drift under peak roof drift (%)									Residual inter-story drift (%)					
	Time (Sec.)	V (kN)	Peak roof drift (%)	Story						Story					
				1	2	3	4	5	6	1	2	3	4	5	6
(a) LA15 ground motion (PGA=0.534 g, 10/50 year)															
6SBRB-S	2.95	7798	1.09	2.00	2.25	1.24	0.56	0.37	0.18	1.04	1.06	0.36	0.29	0.20	0.08
6SBRB-S-SMA	2.97	7977	1.50	2.14	2.77	1.86	1.12	0.74	0.38	0.05	0.16	0.16	0.06	0.07	0.06
6SBRB-V	2.98	7331	1.14	1.97	2.35	1.25	0.59	0.44	0.25	1.06	1.15	0.37	0.26	0.17	0.08
6SBRB-V-SMA	2.99	7560	1.52	2.08	2.86	1.92	1.09	0.75	0.40	0.05	0.16	0.14	0.06	0.07	0.06
6SBRB-2X	2.97	7452	1.09	2.14	2.28	1.10	0.46	0.37	0.20	1.17	1.10	0.35	0.29	0.21	0.10
6SBRB-2X-SMA	2.98	7712	1.49	2.32	2.90	1.68	0.98	0.68	0.36	0.04	0.19	0.10	0.06	0.07	0.07
(b) LA17 ground motion (PGA=0.569 g, 10/50 year)															
6SBRB-S	7.12	7448	0.94	1.67	1.83	1.05	0.50	0.38	0.22	0.74	0.68	0.35	0.25	0.11	0.03
6SBRB-S-SMA	7.12	8053	1.08	1.88	2.19	1.20	0.57	0.38	0.24	0.01	0.00	0.00	0.01	0.00	0.01
6SBRB-V	7.14	7049	0.98	1.74	1.88	1.06	0.51	0.42	0.27	0.82	0.78	0.40	0.22	0.13	0.04
6SBRB-V-SMA	7.12	7993	1.12	1.96	2.30	1.22	0.59	0.41	0.27	0.00	0.04	0.01	0.02	0.01	0.02
6SBRB-2X	7.12	7217	0.97	1.88	1.91	0.99	0.47	0.36	0.22	1.00	0.90	0.39	0.25	0.10	0.04
6SBRB-2X-SMA	7.10	7840	1.08	2.07	2.24	1.09	0.51	0.36	0.21	0.01	0.01	0.01	0.02	0.01	0.02
(c) LA25 ground motion (PGA=0.868 g, 2/50 year)															
6SBRB-S	2.97	7816	1.29	2.10	2.84	1.42	0.79	0.37	0.22	0.94	1.42	0.56	0.27	0.25	0.14
6SBRB-S-SMA	3.03	8993	2.13	3.22	3.88	2.91	1.43	0.87	0.50	0.01	0.22	0.28	0.09	0.11	0.10
6SBRB-V	2.98	7706	1.27	2.03	2.79	1.41	0.74	0.39	0.25	0.88	1.40.	0.54	0.28	0.21	0.15
6SBRB-V-SMA	3.04	8336	2.07	3.08	3.93	2.83	1.39	0.88	0.53	0.05	0.20	0.21	0.06	0.07	0.08
6SBRB-2X	2.98	7630	1.18	2.06	2.60	1.24	0.64	0.36	0.20	0.98	1.47	0.49	0.32	0.26	0.17
6SBRB-2X-SMA	3.03	8506	1.98	3.41	4.08	2.29	1.08	0.74.	0.47	0.08	0.39	0.35	0.10	0.15	0.13
(d) LA27 ground motion (PGA=0.927 g, 2/50 year)															
6SBRB-S	7.22	8718	2.57	4.62	5.17	3.03	1.43	0.75	0.42	2.53	3.20	1.78	0.49	0.20	0.16
6SBRB-S-SMA	7.26	10354	2.01	3.64	3.66	2.42	1.09	0.67	0.45	0.03	0.03	0.09	0.04	0.03	0.05
6SBRB-V	7.24	8503	2.59	4.61	5.25	3.05	1.43	0.77	0.48	2.51	3.25	1.80	0.47	0.19	0.17
6SBRB-V-SMA	7.28	10227	2.20	3.76	3.95	2.83	1.28	0.80	0.57	0.04	0.17	0.19	0.08	0.07	0.08
6SBRB-2X	7.24	8776	2.61	5.28	5.58	2.55	1.16	0.67	0.41	3.28	3.70	1.45	0.38	0.24	0.19
6SBRB-2X-SMA	7.26	10814	2.30	4.25	4.02	3.01	1.28	0.75	0.50	0.08	0.20	0.21	0.09	0.08	0.10

inter-story drifts were mostly generated in the second story. As we also expected, the BRBF models with superelastic SMA bracing systems showed much smaller residual inter-story drifts than those with conventional steel bracing systems, regardless of the type of bracing used. Therefore, excellent recentering ratios were also displayed in the seismic performance of the BRBF models with superelastic SMA bracing systems. The SMA braced-frame models, in particular, had average recentering ratios that exceeded 99% throughout all story levels after the LA17 ground motion, which indicates that they fully reassumed their original shapes. Above all, they displayed a maximum residual inter-story drift less than 0.4%, despite the application of relatively strong seismic excitation (Table 3). From an economic point of view, a residual inter-story drift greater than 0.5% represents the total loss of a frame building (McCormick *et al*., 2008). The steel-braced frame models, even when subjected to 10% in 50 year ground motions, exhibited a maximum residual inter-story drift that was much greater than 0.5%, which would therefore require the reconstruction of the entire building structure rather than the repair of only the damaged parts.

The damage to BRB members subjected to earthquake loads could be adequately evaluated in the same manner by tracing the plastic stress hinge sequence. The plastic stress hinges shown in Figs. 9 and 10 were detected when both BRBF models being compared (6SBRB-S and 6SBRB-S-SMA) encountered the peak roof story drift during nonlinear dynamic analyses performed with long-period ground motions (LA17 and LA27). As can be seen in Figs. 9 (b) and 10 (b), the highest base shear demand on the BRBF model and the peak roof displacement took place at the same time. The stress contour levels were divided into 5 equal sections, based on the nominal strength of base Gr. 50 steel or the superelastic SMA materials in

Table 4. Summary of recentering ratios from nonlinear dynamic analyses

Model ID	V (kN)	Peak roof drift (%)	Recentering ratio=100(Δ_{peak}−$\Delta_{residual}$)/Δ_{peak} (%) Story 1	2	3	4	5	6
(a) LA15 ground motion (PGA=0.534 g, 10/50 year)								
6SBRB-S	7798	1.09	48.24	50.70	55.23	54.64	54.18	54.21
6SBRB-V	7331	1.14	46.34	48.93	53.98	53.95	54.40	54.94
6733SBRB-2X	7452	1.09	45.50	48.87	52.77	51.49	51.00	50.96
Average	**7527**	**1.11**	**46.69**	**49.50**	**53.89**	**53.36**	**53.19**	**53.37**
6SBRB-S-SMA	7977	1.50	97.85	95.84	94.89	94.86	94.52	94.05
6SBRB-V-SMA	7560	1.52	97.78	95.86	94.95	94.90	94.56	94.11
6SBRB-2X-SMA	7712	1.49	98.42	95.72	95.29	95.06	94.59	94.06
Average	**7749**	**1.50**	**98.02**	**95.81**	**95.04**	**94.94**	**94.56**	**94.07**
(b) LA17 ground motion (PGA=0.569 g, 10/50 year)								
6SBRB-S	7448	0.94	55.90	59.42	61.03	59.96	60.67	61.63
6SBRB-V	7049	0.98	53.03	55.92	57.42	57.41	58.34	59.48
6733SBRB-2X	7217	0.97	46.96	50.09	52.31	51.77	53.03	54.05
Average	**7238**	**0.96**	**51.96**	**55.14**	**56.92**	**56.38**	**57.35**	**58.39**
6SBRB-S-SMA	8053	1.08	99.52	99.66	99.69	99.38	99.91	99.96
6SBRB-V-SMA	7993	1.12	99.93	99.10	99.43	99.13	99.02	98.83
6SBRB-2X-SMA	7840	1.08	99.54	99.45	99.32	99.04	98.86	98.62
Average	**7962**	**1.09**	**99.66**	**99.40**	**99.48**	**99.35**	**99.26**	**99.14**
(c) LA25 ground motion (PGA=0.868 g, 2/50 year)								
6SBRB-S	7816	1.29	55.36	52.30	54.20	55.51	54.44	53.85
6SBRB-V	7706	1.27	56.71	52.79	54.80	55.62	55.14	54.60
6733SBRB-2X	7630	1.18	52.34	47.30	50.01	49.92	48.68	47.75
Average	**7717**	**1.25**	**54.80**	**50.80**	**53.00**	**53.68**	**52.75**	**52.07**
6SBRB-S-SMA	8993	2.13	99.58	97.05	95.09	94.90	94.38	93.82
6SBRB-V-SMA	8336	2.07	98.41	97.80	96.27	96.18	95.84	95.37
6SBRB-2X-SMA	8506	1.98	97.61	93.75	91.65	91.57	90.85	90.17
Average	**8612**	**2.06**	**98.53**	**96.20**	**94.34**	**94.21**	**93.69**	**93.12**
(d) LA27 ground motion (PGA=0.927 g, 2/50 year)								
6SBRB-S	8718	2.57	45.12	41.44	41.36	43.82	45.26	45.72
6SBRB-V	8503	2.59	45.59	41.61	41.46	43.97	40.56	46.13
6733SBRB-2X	8776	2.61	37.90	35.79	37.17	39.53	40.59	40.92
Average	**8665**	**2.59**	**42.87**	**39.61**	**40.00**	**42.44**	**43.80**	**44.26**
6SBRB-S-SMA	10354	2.01	99.30	99.87	98.95	98.65	98.46	98.12
6SBRB-V-SMA	10227	2.20	99.06	97.33	96.27	95.97	95.65	95.20
6SBRB-2X-SMA	10814	2.30	98.11	96.58	95.66	95.39	95.04	94.49
Average	**10465**	**2.17**	**98.82**	**97.93**	**96.96**	**96.67**	**96.38**	**95.94**

the BRB members. The extent of the plastic stress hinge, which is depicted as colored solid circles, was determined by examining the fiber stress measured at the integration point.

In the BRB member, the composite segments surrounded by the steel casing and mortar remained in elastic states without buckling. Instead, plastic deformations were concentrated in the extended end connectors that have relatively smaller cross-cross sections. Due to the brace configuration, two pairs of plastic stress hinges consisting of compression and tension were arranged to face each other across the center of each braced bay on both BRB members. A strong ground motion (LA27) induced more plastic stress hinges and more severe failures in the BRBF models than did a weak ground motion (LA17). Overall, the severe plastic failure hinges were mostly distributed at the lower story levels, where the large deformation was concentrated.

The 6SBRB-S frame model under the LA27 ground motion showed plastic stress hinges up to the 5th floor BRB members. The loss of brace capacity due to yielding and the permanent deformation of the steel end connectors

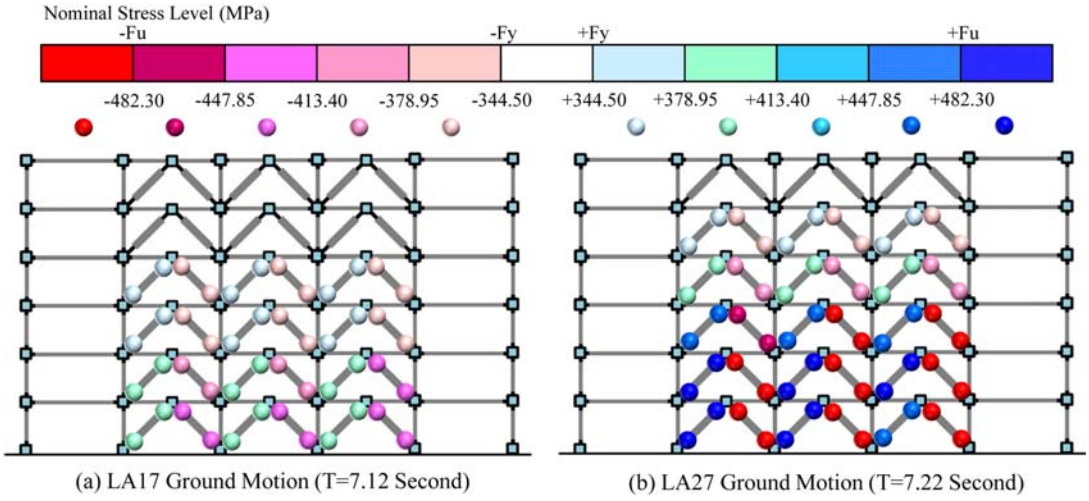

Figure 9. Investigation of plastic stress hinges at peak roof drift (6SBRB-S frame model).

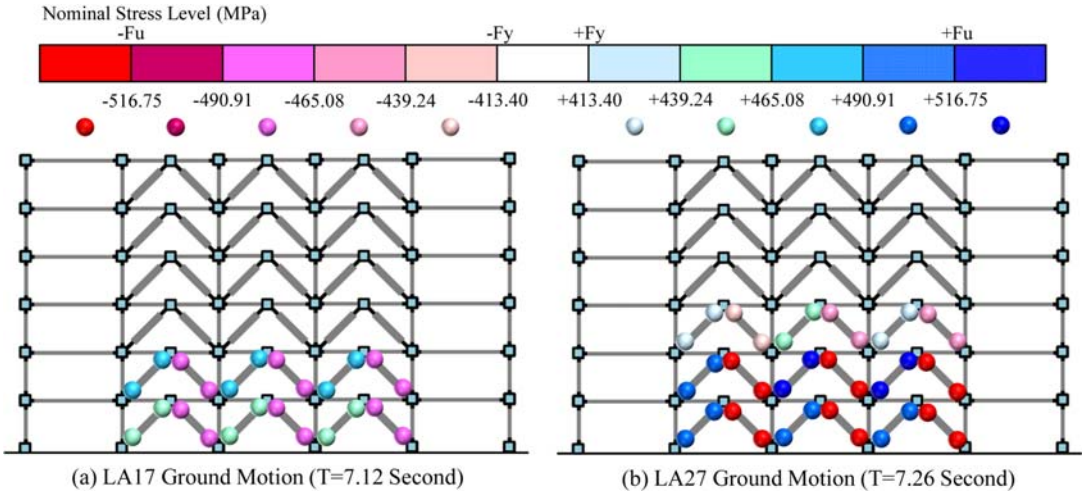

Figure 10. Investigation of plastic stress hinges at peak roof drift (6SBRB-S-SMA frame model).

incurred considerable residual inter-story drifts along the height of the structure. For the case of the 6SBRB-S-SMA frame model, yielding spread only up to the level of the third story. The ability of more BRB members in the 6SBRB-S-SMA frame model to remain elastic can be attributed to the relatively higher level of SMA's post-yield stress, as compared to steel materials. Furthermore, the SMA end connectors with plastic stress hinges were able to return to their original shape after a ground motion. The ability of SMA bracing systems to provide recentering can lead to smaller residual inter-story drifts in a BRB frame structure.

5. Concluding Remarks

Superelastic SMAs have been recently applied to frame design as active control devices because they could recover to original shape upon unloading. The unique behavior of superelastic SMA materials, which can be characterized by a flag-shape hysteresis, provides recentering capability and supplemental damping to the frame structures when these smart materials are utilized in the brace members. To this end, this study has mainly investigated on the seismic response for 6-story BRBF models incorporating superelastic SMA bracing systems. After nonlinear dynamic analyses, the behavior of innovative SMA-braced frames was evaluated, and then compared with that of conventional steel-braced frames in terms of roof story drifts, peak and residual inter-story drifts, recentering ratios, and plastic stress hinge sequences. The end connecting bars in the BRB member are susceptible to yielding under strong earthquake loads because composite BRB segments with larger effective cross-sections are able to remain elastic. The yielding of steel bars in the steel bracing system created permanent deformations in the BRBF models, whereas the use of superelastic SMA bars in the bracing members considerably reduced residual inter-story drifts for both investigated seismic hazard levels. Under the

same ground motion, the end connectors fabricated with superelastic SMA bars preserved more elasticity than those with steel bars as can be seen in the plastic stress hinge sequences, owing to their higher post-yield strength. Therefore, it can be also concluded that the BRBF models with superelastic SMA bracing systems are able to resist more lateral earthquake loads than those with steel bracing systems.

Acknowledgments

This work was supported by the University of Incheon (Incheon National University) Research Grant in 2013. The authors gratefully acknowledge this support. The first author (J.W. Hu) sincerely thanks Prof. Roberto T. Leon for his academic advice and valuable comments when he was a post-doctorate fellow in Georgia Tech.

References

Aiken, I. D., Mahin, S. A., and Uriz, P. (2002). "Large-scale testing of buckling-restrained braced frames." *Proc. Japan Passive Control Symposium,* Tokyo Institute of Technology, Japan, pp. 35-44.

AISC (2001). *Manual of steel construction: Load and Resistance Factor Design (LRFD). 3rd ed.,* American Institute of Steel Construction, Chicago, IL, USA.

ASCE (2005). Minimum design loads for buildings and other structures. *ASCE/SEI No. 7-05*, American Society of Civil Engineers, Reston, VA, USA.

Auricchio, F. and Sacco, E. (1997). "A one-dimensional model for superelastic shape-memory alloys with different properties between martensite and austenite." *Int. J. Non-Linear Mech.,* 32(6), pp. 1101-1114.

Black, C., Makris, N., and Aiken, I. (2002). Component testing, stability analysis and characterization of buckling-restrained braces. *Report No. PEER-2002/08,* Pacific Earthquake Engineering Research Center, University of California, Berkeley, CA, USA.

DesRoches. R., McCormick. J., and Delemont. M. (2004). "Cyclic properties of superelastic shape memory alloy wires and bars." *ASCE J. Struct. Eng.,* 130(1), pp. 38-46.

DesRoches. R. and Delemont. M. (2002). "Seismic retrofit of simply supported bridges using shape memory alloys." *Eng. Struct.*, 24(3), pp. 325-332.

Dolce. M. and Cardone. D. (2001). "Mechanical behaviour of shape memory alloys for seismic applications: 1. Martensite and austenite NiTi bars subjected to torsion." *Int. J. Mech. Sci.*, 43(11), pp. 2631-2656.

Guo, Y., Wang, Z., and Xiao, Y. (2011). "Seismic behavior of buckling restrained braced composite frames." *Adv. Sci. Lett.*, 4(8), pp. 2968-2972.

Hu, J. W. (2008). *Seismic performance evaluations and analyses for composite moment frames with smart SMA PR-CFT connections*. Ph.D. Dissertation, Georgia Institute of Technology, Atlanta, GA, USA.

Hu, J. W. and Leon, R. T. (2011). "Analyses and evaluations for composite-moment frames with SMA PR-CFT connections." *Nonlin. Dyna*., 65(4), DOI: 10.1007/s11071-010-9903-3.

Hu, J. W., Choi, D., and Kim, D. (2012). "Numerical investigation on the cyclic behavior of smart recentering clip-angle connections with superelastic shape memory alloy fasteners." *Proc. Inst. Mech. Eng. Part C: J. Mech. Eng. Sci.,* DOI: 10.1177/0954406212459008.

Hu, J. W., Choi, E., and Leon, R. T. (2011). "Design, analysis, and application of innovative composite PR connections between steel beams and CFT columns Smart Mater." *Struct.,* 20(2), DOI 10.1088/0964-1726/20/2/025019.

Hu, J. W., Kang, Y. S., Choi, D. H., and Park, T. (2010). "Seismic design, performance, and behavior of composite-moment frames with steel beam-to-concrete filled tube column connections." *KSSC Int. J. Steel Struct.*, 10(2), pp. 177-191.

Inoue, K., Sawaisumi, S., and Higashibata, Y. (2001). "Stiffening requirements for unbonded braces encased in concrete panels." *ASCE J. Struct. Eng.*, 127(6), pp. 712-719.

ICC (2006). *International building code 2006 IBC2006 Falls Church*. International Code Council, VA, USA.

Kim, J., Choi, H., and Chung, L. (2004). "Energy-based seismic design of structures with buckling-restrained braces." *Steel Compos. Struct.*, 4(6), pp. 437-452.

Kim, J., Park, J., and Kim, S. (2009). "Seismic behavior factors of buckling-restrained braced frames." *Struct. Eng. Mech.*, 33(3), pp. 261-284.

Mazzoni, S., Mckenna, F., and Fenves, G. L. (2006). *OpenSEES command language manual v. 1.7.3.* Department of Civil Environmental Engineering University of California, Berkeley, CA, USA.

McCormick, J., Aburano, H., Ikenaga, M., and Nakashima, M. (2008). "Permissible residual deformation levels for building structures considering both safety and human elements." *Proc. 14th World Conference Earthquake Engineering*, Beijing, China, Paper No. 05-06-0071.

Ocel, J. M., DesRoches, R., Leon, R. T., Hess, W. G., Krumme, R., Hayes, J. R., and Sweeney, S. (2004). "Steel beam-column connections using shape memory alloys." *ASCE J. Struct. Eng.*, 130(5), pp. 732-740.

Park, T., Hwang, W. S., Leon, R. T., and Hu, J. W. (2011). "Damage evaluation of composite-special moment frames with concrete-filled tube columns under strong seismic loads." *KSCE J. Civil Eng.*, DOI: 10.1007/s12205-011-1225-6.

Sabelli, R. (2004). "Recommended provisions for buckling-restrained braced frames." *AISC Eng. J.*, 41(4), pp. 155-175.

Sabelli, R., Mahin, S. A., and Chang, C. (2003). "Seismic demands on steel braced-frame buildings with buckling-restrained braces." *Eng. Struct.,* 25(5), pp. 655-666.

Somerville, P. G., Smith, N., Punyamurthula, S., and Sun, J. (1997). *Development of ground motion time histories for phase 2 of the FEMA/SAC steel project*. SAC background document, No. SAC/BD 97/04.

Song, G., Ma, N., and Li, H. (2006). "Applications of shape memory alloys in civil structures." *Eng. Struct.*, 28(9), pp. 1266-1274.

Wada, A., Connor, J., Kawai, H., Iwata, M., and Watanabe, A. (1992). "Damage tolerant structures." *Proc. 5th U.S.-Japan Workshop on the Improvement of Structural Design and Construction Practices Applied Technology Council*, ATC-15-4, SanDiego, CA, USA.

Watanabe, A., Hitomi, Y., Yaeki, E., Wada, A., and Fujimoto, M. (1988). "Properties of brace encased in buckling-restraining concrete and steel tube." *Proc. 9th World Conference on Earthquake Engineering, Vol. 5*, Tokyo-Kyoto, Japan, pp. 719-724.